PCCP

ROYAL SOCIETY OF CHEMISTRY

PAPER

View Article Online
View Journal | View Issue

Cite this: *Phys. Chem. Chem. Phys.*, 2023, **25**, 29718

Surface doping of rubrene single crystals by molecular electron donors and acceptors†

Christos Gatsios,[a] Andreas Opitz, *[a] Dominique Lungwitz,[a] Ahmed E. Mansour,[ab] Thorsten Schultz,[b] Dongguen Shin,[a] Sebastian Hammer,[cd] Jens Pflaum,[ce] Yadong Zhang,[f] Stephen Barlow,[f] Seth R. Marder[fg] and Norbert Koch *[ab]

Received 30th July 2023,
Accepted 16th October 2023

DOI: 10.1039/d3cp03640e

rsc.li/pccp

The surface molecular doping of organic semiconductors can play an important role in the development of organic electronic or optoelectronic devices. Single-crystal rubrene remains a leading molecular candidate for applications in electronics due to its high hole mobility. In parallel, intensive research into the fabrication of flexible organic electronics requires the careful design of functional interfaces to enable optimal device characteristics. To this end, the present work seeks to understand the effect of surface molecular doping on the electronic band structure of rubrene single crystals. Our angle-resolved photoemission measurements reveal that the Fermi level moves in the band gap of rubrene depending on the direction of surface electron-transfer reactions with the molecular dopants, yet the valence band dispersion remains essentially unperturbed. This indicates that surface electron-transfer doping of a molecular single crystal can effectively modify the near-surface charge density, while retaining good charge-carrier mobility.

Introduction

Electrical doping in organic semiconductors involves the transfer of electrons between a dopant and the host semiconductor for generating free charge carriers within the host material. The addition of electrons or holes to the semiconductor is accompanied by an energy shift of the Fermi level (electrochemical potential of electrons) relative to the valence and conduction band edges. Manipulating the free charge-carrier concentration, and thus the Fermi level, presents a key strategy for modifying and enhancing the electrical properties of organic semiconductors. Previous efforts employing atomic dopants such as halogens or alkali metals resulted mainly in unstable devices due to the high diffusivity, chemical reactivity, and poor air stability of such dopants.[1–5] In contrast, molecular dopants can be superior doping agents for organic semiconductors due to a number of factors. For instance, their larger size compared to atomic dopants reduces the Coulombic interactions with the contributed charge carriers and the chance of diffusion into the semiconductor's bulk. Also, their moderate sublimation temperature is beneficial for processing and device integrity during fabrication.[6–11]

In parallel with the development of tailored, more efficient dopants, the field of organic semiconductors has advanced noticeably. New classes of thienoacene and pyrene-based organic semiconductors with field-effect charge-carrier mobilities as high as 30 $cm^2 V^{-1} s^{-1}$ were introduced, paving the way for sustainable flexible electronic devices.[12–14] However, the ideal performance of organic electronic devices is severely impacted by high contact resistances and charge-carrier trapping. Several studies indicated that doping can effectively circumvent both obstacles. For example, adding a thin layer of dopants between the metal contact and the semiconductor can effectively reduce the charge injection barriers.[15–17] Passivation of trap states, which can improve the transport characteristics by lowering the threshold voltage, is a further benefit of doping.[18–21] Also, low to moderate doping of the channel can be beneficial as long as the conductivity does not increase at the cost of a decreased current on/off ratio.[22] A previous work by Lüssem *et al.* demonstrated successful doping of pentacene thin films by evaporating thin layers of n-type and p-type dopants, making depletion and inversion operation modes possible.[23] Other works

[a] *Institut für Physik & IRIS Adlershof, Humboldt-Universität zu Berlin, 12489 Berlin, Germany. E-mail: andreas.opitz@hu-berlin.de, norbert.koch@physik.hu-berlin.de*
[b] *Helmholtz-Zentrum Berlin für Materialien und Energie GmbH, 12489 Berlin, Germany*
[c] *Experimentelle Physik VI, Julius-Maximilians-Universität Würzburg, 97074 Würzburg, Germany*
[d] *Center for the Physics of Materials, Departments of Physics and Chemistry, McGill University, Montreal, Qc, Canada*
[e] *Center for Applied Energy Research e.V., Magdalene-Schoch-Str. 3, 97074 Würzburg, Germany*
[f] *Renewable and Sustainable Energy Institute (RASEI), University of Colorado Boulder, Boulder, CO 80309, USA*
[g] *Department of Chemical and Biological Engineering and Department of Chemistry, University of Colorado Boulder, Boulder, CO 80309, USA*

† Electronic supplementary information (ESI) available. See DOI: https://doi.org/10.1039/d3cp03640e

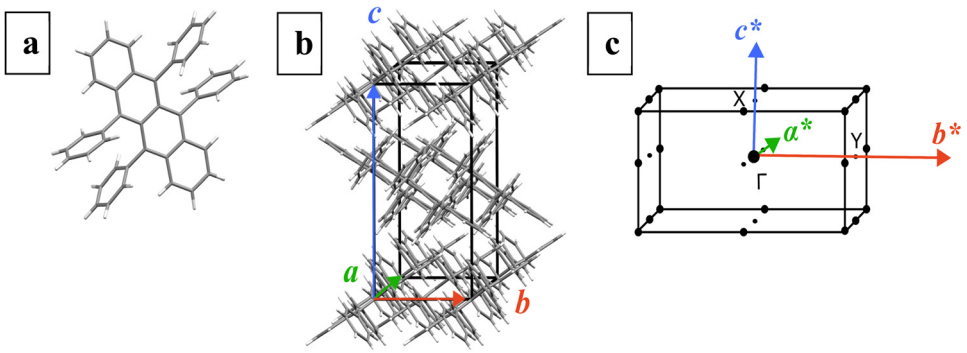

Fig. 1 Molecular structure of rubrene (a). Primitive unit cell of the orthorhombic rubrene single crystal (Cmca) (b). The first Brillouin zone of the reciprocal lattice of rubrene (c). As indicated by the color, each direct lattice vector corresponds to a reciprocal lattice vector. Each direct lattice vector in orthorhombic crystals is parallel to its corresponding reciprocal lattice vector. In the reciprocal space, a dispersive valence band appears along the b^* direction due to the strong wavefunction overlap between the HOMO orbitals along the b crystallographic direction in real space. The Γ point corresponds to the center of the Brillouin zone. The Y and X correspond to high symmetry points at the boundaries of the Brillouin zone.

have also reported the change in the field-effect transistor polarity after doping with molecular electron donors and acceptors.[24–26]

Here, we investigate the surface doping of rubrene single crystals, a benchmark organic semiconductor. As illustrated in Fig. 1a and b, rubrene has a distinct chemical structure and an orthorhombic single-crystalline structure (space group Cmca).[27] Notably, these characteristics facilitate a high hole mobility along the b-axis of its crystal lattice. In fact, previous measurements on rubrene single-crystal field-effect transistors indicate hole mobility values up to 40 $cm^2\ V^{-1}\ s^{-1}$.[28,29] Furthermore, large arrays of high-performance rubrene single-crystal field-effect transistors with mobilities as high as 2.4 $cm^2\ V^{-1}\ s^{-1}$ and large on/off ratios on the order of 10^7, have been fabricated on flexible substrates.[30] For these reasons, rubrene is one of the most relevant technological candidates for organic electronics. The superior electronic properties of rubrene, relative to other molecular semiconductors, are mainly attributed to the formation of a dispersive valence band along the b^* reciprocal lattice vector, which is shown in Fig. 1c. Indeed, density-functional theory calculations indicate a highly dispersive valence band with a bandwidth of 0.4 eV along the Γ–Y path in the Brillouin zone.[31,32] This implies a considerable wavefunction overlap among adjacent rubrene molecules along the ***b***-axis. In line with this, previous angle-resolved photoemission investigations have revealed the valence band dispersion of rubrene.[33–36] Consequently, it is expected that charge transport in rubrene single crystal is essentially mediated by delocalized holes.[37] The current challenge is to control the electronic bands of rubrene through doping without disrupting the single-crystal structure and thus impeding carrier transport.

For this purpose, surface molecular doping can be a more effective strategy than bulk doping. As the electronic properties of organic single crystals ultimately depend on their crystal structure, it is anticipated that bulk doping might have a negative impact. In fact, Hall measurements in bulk-doped rubrene single crystals reported previously by Ohashi *et al.* show decreased Hall mobility. This was attributed to the lattice defects generated by doping that can act as scattering sites, thus reducing the mean free path of the mobile holes.[38] In contrast, introducing a uniform layer of dopants to the surface of rubrene single crystals should not be destructive and could, in principle, alter the near-surface intrinsic electronic character to p-type or n-type.

In this work, we deposited thin layers of two bulky molecular dopants on rubrene single crystals by thermal evaporation in ultrahigh vacuum. One dopant, $Mo(tfd\text{-}CO_2Me)_3$, whose chemical structure is shown in Fig. 2a, has a high electron affinity of 5.0 eV, measured previously by inverse photoemission spectroscopy.[39] As shown schematically in the energy level diagram of Fig. 2c, because the solid-state ionization energy of rubrene lies at almost the same energy, electron transfer is expected to occur from the valence band of rubrene to the lowest unoccupied molecular orbital (LUMO) level of $Mo(tfd\text{-}CO_2Me)_3$. The electron depletion at the surface of rubrene should push the Fermi level towards the valence band, giving the surface a p-type character. Conversely, when an electron-donating molecule is used, the opposite is anticipated. As an electron donor we used cobaltocene ($CoCp_2$), whose chemical structure is shown in Fig. 2b. Cobaltocene has previously been reported to exhibit a low solid-state ionization energy of 4.1 eV.[40] This can trigger an electron transfer from the singly occupied molecular orbital (SOMO) level of $CoCp_2$ to the conduction band of rubrene. The higher electron concentration at the surface of rubrene would move its Fermi level towards the conduction band, resulting in an n-type conductivity behavior.

To test the hypotheses, we performed angle-resolved photoemission spectroscopy (ARPES) measurements on bare and surface-doped rubrene single crystals with the above-mentioned molecular electron donors and acceptors. ARPES allows direct observation of the electronic bands, and we could directly disclose the effect of surface doping on the valence band of rubrene. Our results underpin this non-destructive doping approach, in which the dopants are adsorbed on the surface of rubrene without disrupting its single-crystalline structure.

Experiment

Rubrene single crystals were grown *via* horizontal physical vapor transport.[41,42] For this purpose, a steep temperature

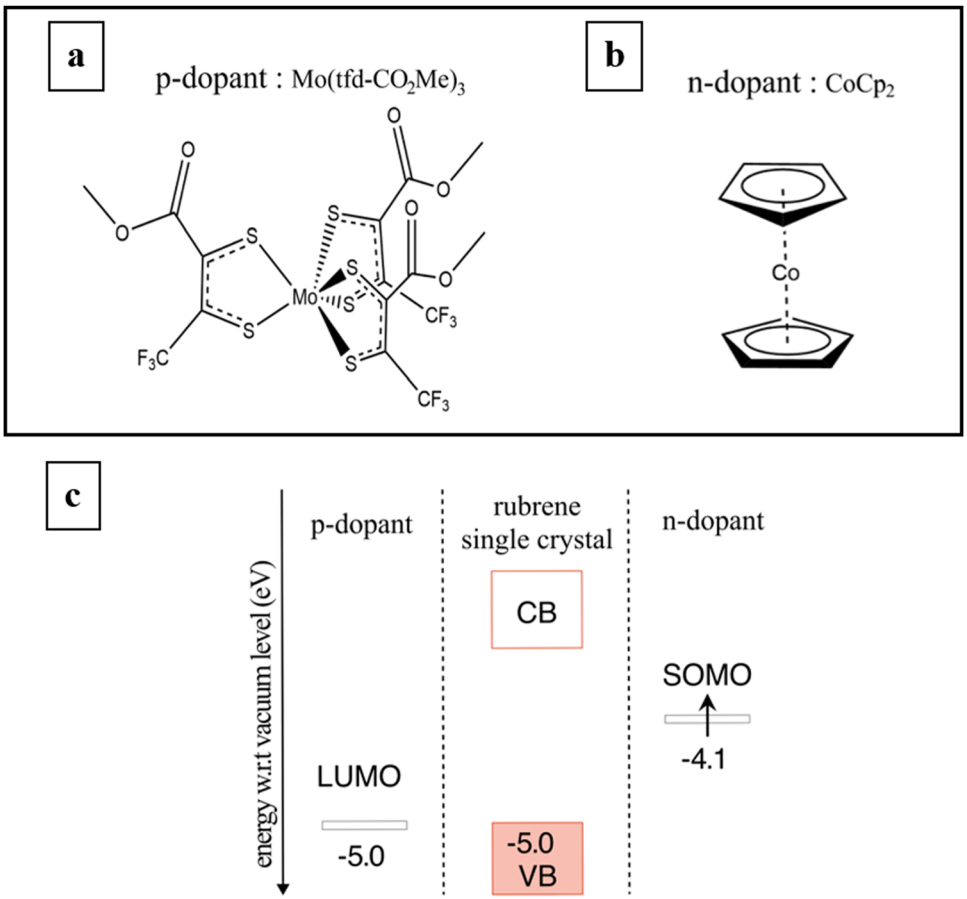

Fig. 2 Chemical structures of $Mo(tfd\text{-}CO_2Me)_3$ (a) and $CoCp_2$ (b) molecules. The electronic energy levels for the LUMO and SOMO of the p-dopant and n-dopant, respectively, are shown with respect to the vacuum level (c). In the case rubrene single crystal wider boxes are used to represent the valence (VB) and conduction bands (CB). The valence band maximum is measured in this work and found to be −5.0 eV. The energy of the conduction band minimum is tentatively positioned approximately 2.8 eV closer to the vacuum level, taking into account the band gap of previously measured rubrene thin films by inverse photoemission spectroscopy.[58] This placement provides only a rough representation as it applies data from thin films to our current study on single crystals.

gradient is applied across a fused silica glass tube which is located in a furnace. Simultaneously, a 30 sccm N_2 (6 N purity) inert gas flow is applied. On the hot side of the furnace, the starting material, *ca.* 105 mg of purified rubrene powder, is placed and sublimed at 335 °C over 48 h. The sublimed material is transported along the temperature gradient to the cold side, where it recrystallizes, yielding plate-like single crystals with a lateral extension of up to 5 mm. The as-grown crystals were slowly cooled down over 8 h to minimize thermal stress.

Prior to the photoemission experiments, the rubrene single crystals were attached to copper substrates using silver paste to allow sample grounding. Photoemission experiments were performed at the LowDosePES end-station of the BESSY II PM4 beamline of the Helmholtz Zentrum Berlin für Materialien und Energie GmbH (HZB). PM4 is equipped with an angle-resolved time-of-flight (ArTOF) spectrometer that collects the emitted electrons at a broad solid angle of up to 30°. The pulsed excitation source required by the ArTOF analyzers is suitable for investigating radiation sensitive samples such as organics.[43] All experiments were conducted at ambient temperature and in ultrahigh vacuum (10^{-9} mbar). The excitation energy was set to 35 eV corresponding to a short photoelectron mean free path (5–10 Å), for which only electrons from rubrene's uppermost layers contribute to the signal. The experimental setup provides a 20 meV energy resolution and a 0.09° angular resolution.

We measured two rubrene single-crystal samples, the electronic band structures of which were essentially identical (Fig. S1, ESI†). A minor discrepancy of approximately 50 meV in the binding energy position of the valence peaks between the two samples can be observed by the results of the quantitative analysis on the valence peaks (Table S1, ESI†). This discrepancy could potentially be attributed to the inherent uncertainty associated with the measurements of samples of varying thicknesses, or to minute variations in crystal growth conditions within the same or different production batches. During the measurement, consecutive energy-distribution curves (EDCs) recorded over equal time durations revealed the impact of sample charging: broadening and shifting of the HOMO peak

towards higher binding energy. In photoemission from materials having low conductivity, such as organics, the buildup of a positive surface charge due to the removal of electrons is typically a hurdle for the accurate interpretation of photoemission spectra. But it can usually be compensated by taking advantage of their photoconductivity induced by an external source of light.[44] In our case, we used a continuous wave laser of 473 nm wavelength to constantly illuminate the sample. To neutralize the radiation induced charging, a nominal laser power density of 0.3 mW cm^{-2} was required (Fig. S2, ESI†).

Surface doping was achieved *in situ* by thermally evaporating the molecular dopants on bare rubrene single crystals. p-Doping was achieved by depositing a thin layer of $Mo(tfd\text{-}CO_2Me)_3$ at a constant evaporation rate of 0.1 Å s^{-1}, as measured by a quartz crystal microbalance. The final nominal thickness of the molecular layer was 1.5 nm. In the case of the n-doping with $CoCp_2$ the film thickness could not be determined due to the high volatility of $CoCp_2$. Instead, we observed the changes in rubrene's valence band structure throughout three successive evaporations, each of an increasing duration.

Results and discussion

I. Band structure of the bare rubrene single crystal

In Fig. 3a–d, we show the angle-resolved EDCs and the corresponding 2D spectra of bare rubrene along the *Γ–Y* and *Γ–X* directions of the Brillouin zone, respectively. Along the *Γ–X* direction, Fig. 3b and d, there is no clear indication of dispersive features in the valence region. In the *Γ–Y* direction,

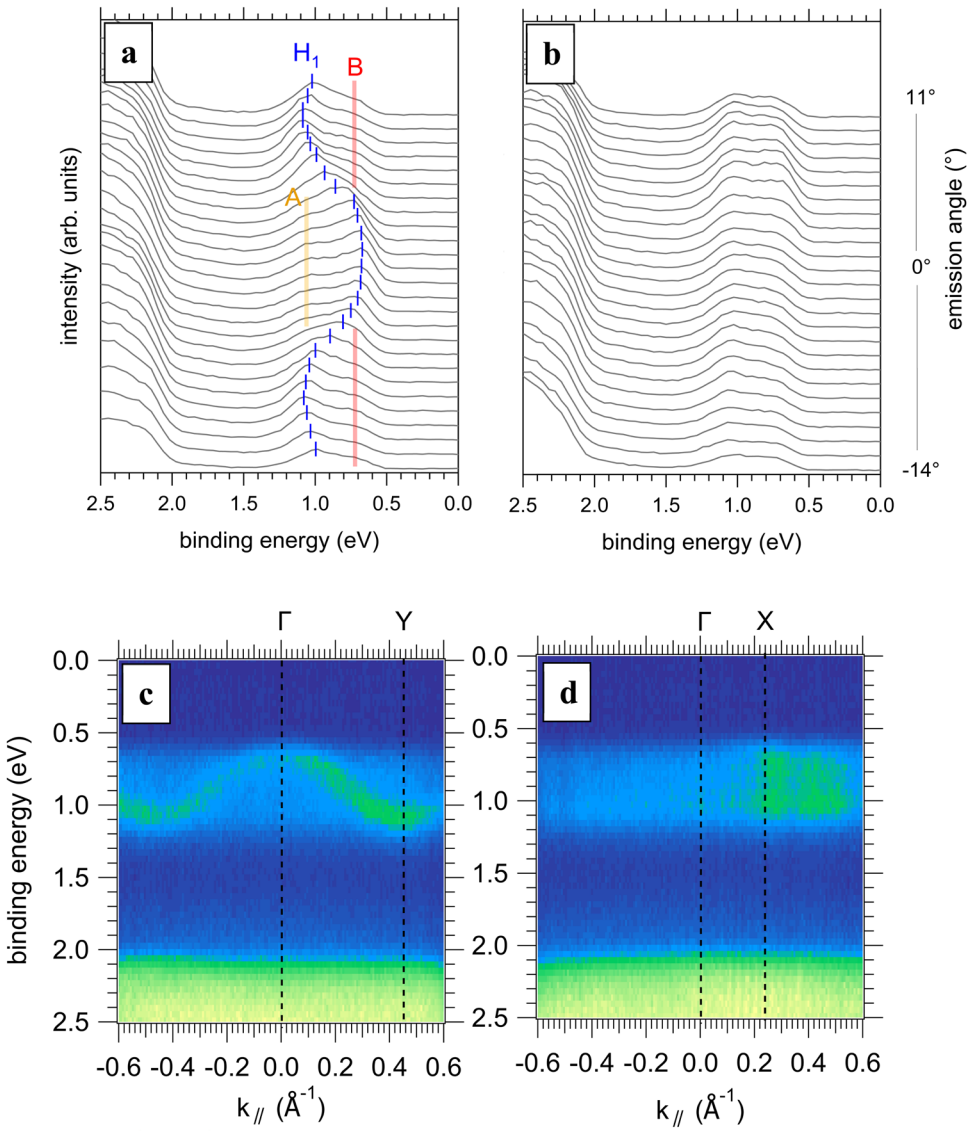

Fig. 3 Angle-resolved EDCs along *Γ–Y* (a), and *Γ–X* (b) paths in the Brillouin zone. The short blue lines indicate the peak position of the dispersive H_1 peak and the yellow and red lines show the non-dispersive A and B satellite features of the spectrum. The respective 2D spectra of the *Γ–Y* (c) and *Γ–X* (d) show valence band of rubrene. The black dashed lines indicate the positions of the *Γ*, *Y* and *X* high symmetry points of the Brillouin zone.

Fig. 3a and c, there is a visible dispersive peak (H_1), which can be associated with the HOMO derived valence band of rubrene single crystals, as demonstrated in earlier experimental and theoretical studies.[31–34] The observed band structure should be consistent with similarly prepared crystals that have been structurally characterized previously.[45] The maximum of the valence band is at the Γ point, 0.64 eV below the Fermi level, determined by the peak maximum of H_1 at the Γ point. Notably, the Γ–Y direction shows two additional features, A and B, which appear at fixed binding energy positions below the band maximum and have also been observed in prior ARPES measurements.[33,34,46] Experimental and theoretical works on rubrene single crystals have previously demonstrated the appearance of a second dispersive band along the Γ–Y direction. This was attributed to the presence of two inequivalent molecules within the surface unit cell corresponding to the *ab* plane.[32,33,47]This can explain the A feature below H_1. A peak analysis of the EDC at the Γ point revealed that the energy separation between H_1 and A is roughly 0.3 eV (Fig. S3 and Table S1, ESI†). The observed energy separation does not fully match the theoretical value of 0.20 eV, although such a difference is expected when density-functional theory fails to capture the correct many-electron correlation effects in the excited system. In fact, it has been demonstrated before for pentacene that molecular vibration and the presence of disorder can explain the greater separation between the two HOMO-derived bands.[48]

Additionally, the origin of feature B is unexplained by previous density-functional theory calculations of the band structure of rubrene. This feature presents as a *k*-independent uniform background, broadening the H_1 peak. This can be indicative of non-direct transitions as a result of photoelectron scattering events with molecular vibrations, phonons or surface impurities such as residual water or oxygen due to the prior exposure of the single crystals to ambient conditions.[49] The weakening of momentum conservation due to scattering enables transitions from other regions of the Brillouin zone. As a result, every *k*-resolved spectrum can obtain an incoherent background intensity corresponding to the averaging of the density of states to a certain degree over the Brillouin zone. Specifically, according to the previous works of White *et al.* the total *k*-resolved photoelectron spectrum ($I_{tot}(k,E)$) can be described as the sum of a coherent spectrum associated with direct electronic transitions ($I_{coh}(k,E)$), and an incoherent background mentioned above which relates to the non-direct transitions ($I_{incoh}(k,E)$):

$$I_{tot}(k,E) = W \cdot I_{coh}(k,E) + I_{incoh}(k,E) \quad (1)$$

here, W represents the Debye–Waller factor which should be related to the mean square displacements of the molecules at the surface.[50,51] For the reasons mentioned above, we can assume that the incoherent component resembles the *k*-integrated EDC obtained in our experiments. Consequently, we can subtract it from every *k*-resolved EDC to qualitatively estimate the coherent spectral intensity despite not knowing W. This background subtraction method, results in sharper 2D spectra, simplifying the quantitative analysis for determining the intrinsic band parameters (Fig. S4 and S5 ESI†). The band parameters can be determined by approximating the HOMO-derived valence band with the energy dispersion relation of the 1D tight-binding model:

$$E_B(k) = E_C + 2t \cdot \cos(ak) \quad (2)$$

where E_B is the electron's binding energy, k the electron's momentum, E_C the energy of the center of the valence band, t the transfer integral, and a the lattice constant. Moreover, the hole effective mass at the Γ point, m^*_{TB}, is given by:

$$m^*_{TB} = -\frac{\hbar^2}{2ta^2} \quad (3)$$

The above relations are used for the analysis of band structure properties further below.

II. Surface molecular doping

The 2D intensity maps of bare and surface-doped rubrene are depicted in Fig. 4a–d. In the case of Mo(tfd-CO_2Me)$_3$, the deposited layer of molecular acceptors shifted the valence band of rubrene 90 meV toward the Fermi level, as seen in Fig. 4a and b. In contrast, the molecular donor $CoCp_2$ induced a 140 meV shift of the valence band in the opposite direction, as shown in Fig. 4c and d. In either case, the shift of the valence band can be attributed to electron-transfer reactions at the interface between the dopants and rubrene. In particular, the deposited layer of molecular acceptors triggers an electron transfer from the highest occupied valence states of rubrene close to the interface to the LUMO of Mo(tfd-CO_2Me)$_3$ in order to achieve electronic equilibrium. The redistribution of charges (*i.e.*, space-charge accumulation) generates an electric field close to the interface, which bends the valence band upwards and is associated with an increased concentration of holes at the surface of rubrene. Conversely, the deposition of donor molecules causes an electron transfer from the SOMO of $CoCp_2$ to the lowest unoccupied states of rubrene. The increased concentration of electrons at the surface of rubrene induced a downward bending of the valence band.

To further corroborate the impact of deposition on the surface, atomic force microscopy (AFM) measurements were conducted in ambient conditions. These measurements revealed evident changes in the surface topography of single-crystal rubrene after doping. Following the deposition of the p-dopant Mo(tfd-CO_2Me)$_3$, pronounced island growth was observed. In contrast, the introduction of the n-dopant CoCp2 led to the formation of less dense islands (Fig. S6, ESI†). In both cases, sub-monolayer coverage is achievable.

In addition, we observed that the valence band along the Γ–X direction exhibited similar shifts due to surface doping (as shown in Fig. S7 of the ESI†). This observation suggests that the doping process likely induced a uniform charge distribution on the surface, leading to a concurrent shift in all electronic states. Assuming that the induced charge carriers at the band edges behave as free particles and that they obey Boltzmann statistics we can roughly estimate the induced concentration of

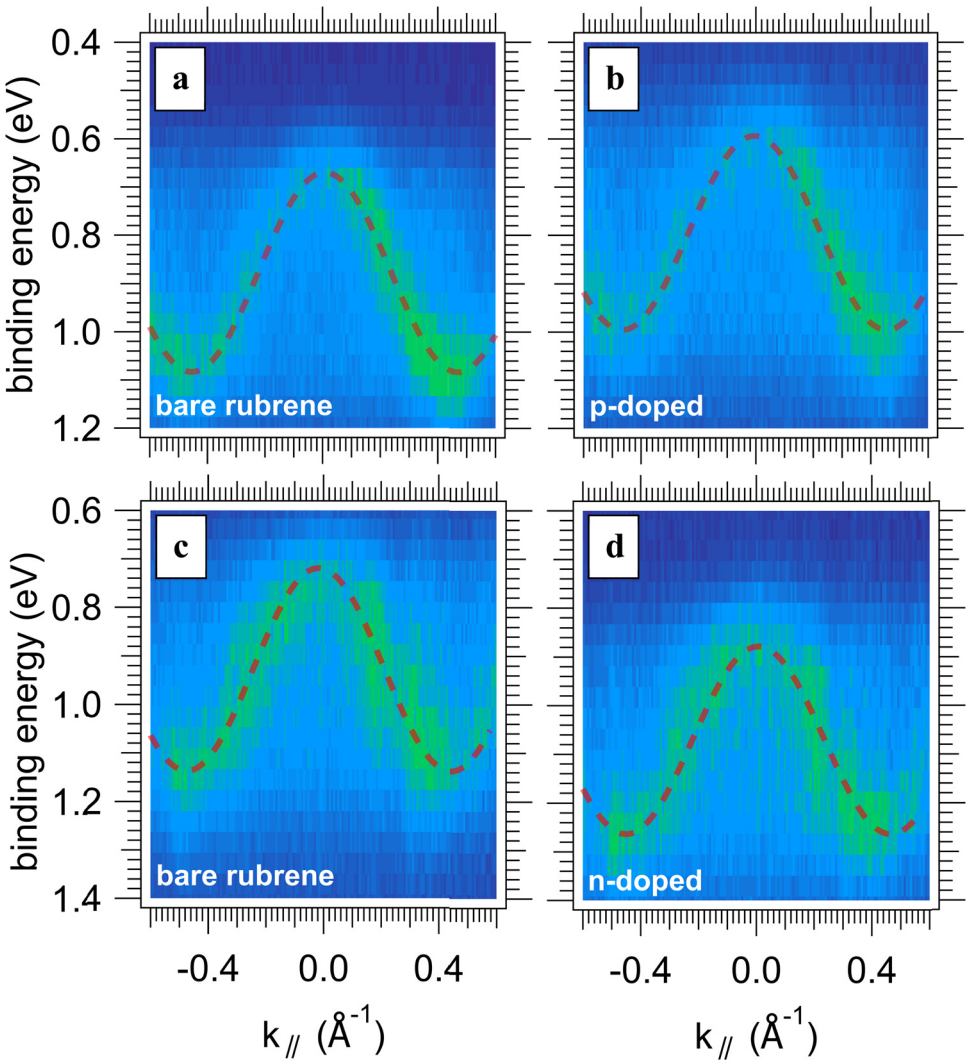

Fig. 4 2D spectra of the bare (undoped) rubrene (a) and (c), surface p-doped rubrene (b) and surface n-doped rubrene (d). The red curve represents the least-square fit of the valence band approximated by the 1D tight-binding dispersion relation.

holes by the following expression:

$$\frac{p_f}{p_i} = \exp\left[-\frac{\Delta E_V}{k_b T}\right] \quad (4)$$

where p_i is the initial concentration of holes for the undoped rubrene, p_f the final concentration of holes after surface doping and ΔE_V the energy shift of the valence band.[52] Given that at room temperature the thermal energy is $k_b T = 25$ meV, then the valence-band energy shifts of −90 meV and 140 meV could effectively modulate the hole concentration at the surface by up to two orders of magnitude. Most importantly, it appears that the surface molecular doping had no apparent effect on the shape of the rubrene valence band. A quantitative analysis, the results of which are listed in Table 1, revealed that the band parameters, transfer integral, and hole effective mass, remain essentially constant. Therefore, it is reasonable to assume that the deposition of Mo(tfd-CO_2Me)$_3$ and $CoCp_2$, and the induced charge concentrations, do not result in structural deformation of the surface lattice of rubrene nor in anisotropic charge-carrier distribution along certain directions.

The magnitude of the valence band shifts, related to doping efficiency, is noteworthy, as it does not appear to be strictly determined by the energy offsets between the frontier energy levels of rubrene and the dopants. One might expect larger changes, even for such small energy differences. Several distinct and interrelated factors may explain this situation. First,

Table 1 Band parameters of 1D-tight binding approximation where (E_C) the center of the valence band, (ΔE_C) the shift of the valence band center after doping, (a) lattice parameter corresponding to *b* crystallographic axis of rubrene single crystal, (*t*) transfer integral and (m^*_{TB}) hole effective mass

	E_C (eV)	ΔE_C (meV)	a (Å)	t (meV)	$\lvert m^*_{TB}\rvert$ (m_0)
Bare rubrene	0.88 ± 0.01	—	6.8 ± 0.1	103 ± 10	0.8 ± 0.1
p-Doped	0.79 ± 0.01	−90 ± 10	6.8 ± 0.1	100 ± 10	0.8 ± 0.1
Bare rubrene	0.93 ± 0.01	—	6.9 ± 0.1	105 ± 10	0.7 ± 0.1
n-Doped	1.07 ± 0.01	140 ± 10	6.9 ± 0.1	101 ± 10	0.8 ± 0.1

the small shift in the case of the p-dopant could be related to the low dopant concentration on the surface, as indicated by the small signals observed in the X-ray photoemission spectra (Fig. S8, ESI†). Second, materials inherently contain native defects, the origin, concentration, and spatial distribution of which largely depend on the crystal growth conditions and the post-treatment of the crystals after growth. These native defects can generate an intra-bandgap density of states, acting as electron donors or acceptors, and consequently, compensating for further doping of the surface. In this scenario, the Fermi level becomes pinned by the defect states, causing the valence band to be fixed at a certain position, irrespective of the dopant concentrations.[53–55] Lastly, unfavorable intermolecular interactions at the interface, coupled with disadvantageous intermolecular geometries, can notably alter the energetics of the donating and accepting energy levels. This could create energy barriers that hinder charge-carrier hopping across the interface.[56,57]

Conclusions

In conclusion, our photoemission results demonstrate that surface doping by thermal evaporation of molecular thin layers can indeed change the intrinsic electronic character of rubrene single crystal surfaces to more n-type or p-type. This is attributed to the observed shifts of the rubrene valence band relative to the Fermi level. Importantly, the doping is accomplished without disrupting the surface structure of single-crystal rubrene, a prerequisite to preserving the HOMO-derived valence band. A next step could be charge-transport measurements to test how the surface molecular doping of rubrene single crystals affects device characteristics. Furthermore, in order to comprehend the magnitude of the observed shifts and identify specific routes for the efficient doping of organic semiconductors it is necessary to fully understand the reasons that may limit the surface molecular doping of rubrene. This could involve the use of different molecular dopants and a systematic investigation of both the microscopic interactions between the semiconductor host and the dopants as well as the potential thermodynamic limitations of doping organic semiconductors containing native defects. These points should form the basis of our future studies.

Author contributions

C. G., A. O., D. L., A. E. M., T. S., D. S. performed photoemission measurements. S. H. and J. P. grew rubrene single crystals, and Y. Z. synthesized dopants. A. O., J. P., S. B., S. R. M., N. K. supervised the project and provided resources. C. G. and A. O. wrote the original draft, and all authors contributed to reviewing and editing the final manuscript.

Conflicts of interest

There are no conflicts of interest to declare.

Acknowledgements

We gratefully acknowledge the beamline scientists of PM4 endstation Dr. Erika Giangrisostomi and Dr. Ruslan Ovsyannicov for their kind support in the course of the ArTOF experiments. We also thank Dr. Patrick Amsalem and Dr. Ross Warren for the insightful discussions. This project has received funding from the DFG project 239543752 and the European Union's Horizon 2020 research and innovation programme under the Marie Skłodowska-Curie grant agreement No. 811284 (UHMOB). S. H. gratefully acknowledges funding from the German Research Foundation (DFG) within project 490894053. S. H. and J. P. acknowledge financial support by the Bavarian State Ministry of Science, Research, and the Arts (Collaborative Research Network 'Solar Technologies Go Hybrid'). Y. Z, S. B., and S. R. M. thank the National Science Foundation for support through the DMREF program (DMR-1729737).

References

1 Y. Yamamoto, K. Yoshino and Y. Inuishi, Electrical Properties of Phthalocyanine-Halogen Complexes, *J. Phys. Soc. Jpn.*, 1979, **47**, 1887–1891, DOI: 10.1143/JPSJ.47.1887.
2 T. Minakata, I. Nagoya and M. Ozaki, Highly ordered and conducting thin film of pentacene doped with iodine vapor, *J. Appl. Phys.*, 1991, **69**, 7354–7356, DOI: 10.1063/1.347594.
3 A. Ali Benamara, M. Galtier and A. Montaner, N doping of polyacetylene, *Synth. Met.*, 1991, **41**, 45–48, DOI: 10.1016/0379-6779(91)90993-F.
4 G. Parthasarathy, C. Shen, A. Kahn and S. R. Forrest, Lithium doping of semiconducting organic charge transport materials, *J. Appl. Phys.*, 2001, **89**, 4986–4992, DOI: 10.1063/1.1359161.
5 R. Di Pietro and H. Sirringhaus, High resolution optical spectroscopy of air-induced electrical instabilities in n-type polymer semiconductors, *Adv. Mater.*, 2012, **24**, 3367–3372, DOI: 10.1002/adma.201200829.
6 J. H. Oh, P. Wei and Z. Bao, Molecular n-type doping for air-stable electron transport in vacuum-processed n-channel organic transistors, *Appl. Phys. Lett.*, 2010, **97**, 243305, DOI: 10.1063/1.3527972.
7 C. Murawski, C. Fuchs, S. Hofmann, K. Leo and M. C. Gather, Alternative p-doped hole transport material for low operating voltage and high efficiency organic light-emitting diodes, *Appl. Phys. Lett.*, 2014, **105**, 113303, DOI: 10.1063/1.4896127.
8 B. Lüssem, M. Riede and K. Leo, Doping of organic semiconductors, *Phys. Status Solidi A*, 2013, **210**, 9–43, DOI: 10.1002/pssa.201228310.
9 I. Salzmann and G. Heimel, Toward a comprehensive understanding of molecular doping organic semiconductors (review), *J. Electron Spectros. Relat. Phenom.*, 2015, **204**, 208–222, DOI: 10.1016/j.elspec.2015.05.001.
10 I. Salzmann, G. Heimel, M. Oehzelt, S. Winkler and N. Koch, Molecular Electrical Doping of Organic Semiconductors: Fundamental Mechanisms and Emerging Dopant Design

Rules, *Acc. Chem. Res.*, 2016, **49**, 370–378, DOI: 10.1021/acs.accounts.5b00438.

11 I. E. Jacobs and A. J. Moulé, Controlling Molecular Doping in Organic Semiconductors, *Adv. Mater.*, 2017, **29**, 1703063, DOI: 10.1002/adma.201703063.

12 M. J. Kang, I. Doi, H. Mori, E. Miyazaki, K. Takimiya, M. Ikeda and H. Kuwabara, Alkylated dinaphtho[2,3-*b*:2′,3′-*f*]thieno[3,2-*b*]thiophenes (Cn-DNTTs): organic semiconductors for high-performance thin-film transistors, *Adv. Mater.*, 2011, **23**, 1222–1225, DOI: 10.1002/adma.201001283.

13 T. Yamamoto and K. Takimiya, Facile synthesis of highly π-extended heteroarenes, dinaphtho[2,3-*b*:2′,3′-*f*]chalcogenopheno[3,2-*b*]chalcogenophenes, and their application to field-effect transistors, *J. Am. Chem. Soc.*, 2007, **129**, 2224–2225, DOI: 10.1021/ja068429z.

14 K. Takimiya, K. Bulgarevich, M. Abbas, S. Horiuchi, T. Ogaki, K. Kawabata and A. Ablat, ''Manipulation'' of Crystal Structure by Methylthiolation Enabling Ultrahigh Mobility in a Pyrene-Based Molecular Semiconductor, *Adv. Mater.*, 2021, **33**, 2102914, DOI: 10.1002/adma.202102914.

15 A. A. Günther, M. Sawatzki, P. Formánek, D. Kasemann and K. Leo, Contact Doping for Vertical Organic Field-Effect Transistors, *Adv. Funct. Mater.*, 2016, **26**, 768–775, DOI: 10.1002/adfm.201504377.

16 T. Minari, P. Darmawan, C. Liu, Y. Li, Y. Xu and K. Tsukagoshi, Highly enhanced charge injection in thienoacene-based organic field-effect transistors with chemically doped contact, *Appl. Phys. Lett.*, 2012, **100**, 093303, DOI: 10.1063/1.3690949.

17 S. Singh, S. K. Mohapatra, A. Sharma, C. Fuentes-Hernandez, S. Barlow, S. R. Marder and B. Kippelen, Reduction of contact resistance by selective contact doping in fullerene n-channel organic field-effect transistors, *Appl. Phys. Lett.*, 2013, **102**, 153303, DOI: 10.1063/1.4802237.

18 S. Olthof, S. Mehraeen, S. K. Mohapatra, S. Barlow, V. Coropceanu, J. L. Brédas, S. R. Marder and A. Kahn, Ultralow doping in organic semiconductors: evidence of trap filling, *Phys. Rev. Lett.*, 2012, **109**, 176601, DOI: 10.1103/PhysRevLett.109.176601.

19 J. Soeda, Y. Hirose, M. Yamagishi, A. Nakao, T. Uemura, K. Nakayama, M. Uno, Y. Nakazawa, K. Takimiya and J. Takeya, Solution-crystallized organic field-effect transistors with charge-acceptor layers: high-mobility and low-threshold-voltage operation in air, *Adv. Mater.*, 2011, **23**, 3309–3314, DOI: 10.1002/adma.201101027.

20 P. Wei, J. H. Oh, G. Dong and Z. Bao, Use of a 1*H*-benzoimidazole derivative as an n-type dopant and to enable air-stable solution-processed n-channel organic thin-film transistors, *J. Am. Chem. Soc.*, 2010, **132**, 8852–8853, DOI: 10.1021/ja103173m.

21 M. P. Hein, A. A. Zakhidov, B. Lüssem, J. Jankowski, M. L. Tietze, M. K. Riede and K. Leo, Molecular doping for control of gate bias stress in organic thin film transistors, *Appl. Phys. Lett.*, 2014, **104**, 013507, DOI: 10.1063/1.4861168.

22 Y. Abe, T. Hasegawa, Y. Takahashi, T. Yamada and Y. Tokura, Control of threshold voltage in pentacene thin-film transistors using carrier doping at the charge-transfer interface with organic acceptors, *Appl. Phys. Lett.*, 2005, **87**, 1–3, DOI: 10.1063/1.2099540.

23 B. Lüssem, M. L. Tietze, H. Kleemann, C. Hoßbach, J. W. Bartha, A. Zakhidov and K. Leo, Doped organic transistors operating in the inversion and depletion regime, *Nat. Commun.*, 2013, **4**, 1–6, DOI: 10.1038/ncomms3775.

24 D. Khim, K. J. Baeg, M. Caironi, C. Liu, Y. Xu, D. Y. Kim and Y. Y. Noh, Control of ambipolar and unipolar transport in organic transistors by selective inkjet-printed chemical doping for high performance complementary circuits, *Adv. Funct. Mater.*, 2014, **24**, 6252–6261, DOI: 10.1002/adfm.201400850.

25 B. Sun, W. Hong, E. S. Thibau, H. Aziz, Z. H. Lu and Y. Li, Polyethylenimine (PEI) As an Effective Dopant to Conveniently Convert Ambipolar and p-Type Polymers into Unipolar n-Type Polymers, *ACS Appl. Mater. Interfaces*, 2015, **7**, 18662–18671, DOI: 10.1021/acsami.5b05097.

26 X. Cheng, Y. Y. Noh, J. Wang, M. Tello, J. Frisch, R. P. Blum, A. Vollmer, J. P. Rabe, N. Koch and H. Sirringhaus, Controlling electron and hole charge injection in ambipolar organic field-effect transistors by self-assembled monolayers, *Adv. Funct. Mater.*, 2009, **19**, 2407–2415, DOI: 10.1002/adfm.200900315.

27 O. D. Jurchescu, A. Meetsma and T. T. M. Palstra, Low-temperature structure of rubrene single crystals grown by vapor transport, *Electrochem. Solid-State Lett.*, 2006, **9**, 330–334, DOI: 10.1107/S0108768106003053/BK5027CP995HSUP9.FCF.

28 J. Takeya, M. Yamagishi, Y. Tominari, R. Hirahara, Y. Nakazawa, T. Nishikawa, T. Kawase, T. Shimoda and S. Ogawa, Very high-mobility organic single-crystal transistors with in-crystal conduction channels, *Appl. Phys. Lett.*, 2007, **90**, 102120, DOI: 10.1063/1.2711393.

29 W. Xie, K. A. McGarry, F. Liu, Y. Wu, P. P. Ruden, C. J. Douglas and C. D. Frisbie, High-mobility transistors based on single crystals of isotopically substituted rubrene-d_{28}, *J. Phys. Chem. C*, 2013, **117**, 11522–11529, DOI: 10.1021/jp402250v.

30 A. L. Briseno, S. C. B. Mannsfeld, M. M. Ling, S. Liu, R. J. Tseng, C. Reese, M. E. Roberts, Y. Yang, F. Wudl and Z. Bao, Patterning organic single-crystal transistor arrays, *Nature*, 2006, **444**, 913–917, DOI: 10.1038/nature05427.

31 D. A. Da Silva Filho, E. G. Kim and J. L. Brédas, Transport properties in the rubrene crystal: electronic coupling and vibrational reorganization energy, *Adv. Mater.*, 2005, **17**, 1072–1076, DOI: 10.1002/adma.200401866.

32 S. Yanagisawa, Y. Morikawa and A. Schindlmayr, HOMO band dispersion of crystalline rubrene: effects of self-energy corrections within the GW approximation, *Phys. Rev. B: Condens. Matter Mater. Phys.*, 2013, **88**, 1–7, DOI: 10.1103/PhysRevB.88.115438.

33 S. I. MacHida, Y. Nakayama, S. Duhm, Q. Xin, A. Funakoshi, N. Ogawa, S. Kera, N. Ueno and H. Ishii, Highest-occupied-molecular-orbital band dispersion of rubrene single crystals as observed by angle-resolved ultraviolet photoelectron spectroscopy, *Phys. Rev. Lett.*, 2010, **104**, 156401, DOI: 10.1103/PhysRevLett.104.156401.

34 A. Vollmer, R. Ovsyannikov, M. Gorgoi, S. Krause, M. Oehzelt, A. Lindblad, N. Mrtensson, S. Svensson,

P. Karlsson, M. Lundvuist, T. Schmeiler, J. Pflaum and N. Koch, Two dimensional band structure mapping of organic single crystals using the new generation electron energy analyzer ARTOF, *J. Electron Spectros. Relat. Phenom.*, 2012, **185**, 55–60, DOI: 10.1016/j.elspec.2012.01.003.

35 Y. Nakayama, Y. Uragami, S. Machida, K. R. Koswattage, D. Yoshimura, H. Setoyama, T. Okajima, K. Mase and H. Ishii, Full picture of valence band structure of rubrene single crystals probed by angle-resolved and excitation-energy-dependent photoelectron spectroscopy, *Appl. Phys. Express*, 2012, **5**, 1–4, DOI: 10.1143/APEX.5.111601.

36 J. Nitta, K. Miwa, N. Komiya, E. Annese, J. Fujii, S. Ono and K. Sakamoto, The actual electronic band structure of a rubrene single crystal, *Sci. Rep.*, 2019, **9**, 1–7, DOI: 10.1038/s41598-019-46080-4.

37 M. Fischer, M. Dressel, B. Gompf, A. K. Tripathi and J. Pflaum, Infrared spectroscopy on the charge accumulation layer in rubrene single crystals, *Appl. Phys. Lett.*, 2006, **89**, 182103, DOI: 10.1063/1.2370743/919315.

38 C. Ohashi, S. Izawa, Y. Shinmura, M. Kikuchi, S. Watase, M. Izaki, H. Naito and M. Hiramoto, Hall Effect in Bulk-Doped Organic Single Crystals, *Adv. Mater.*, 2017, **29**, 1605619, DOI: 10.1002/adma.201605619.

39 A. Dai, Y. Zhou, A. L. Shu, S. K. Mohapatra, H. Wang, C. Fuentes-Hernandez, Y. Zhang, S. Barlow, Y. L. Loo, S. R. Marder, B. Kippelen and A. Kahn, Enhanced charge-carrier injection and collection *via* lamination of doped polymer layers p-doped with a solution-processible molybdenum complex, *Adv. Funct. Mater.*, 2014, **24**, 2197–2204, DOI: 10.1002/adfm.201303232.

40 C. K. Chan, F. Amy, Q. Zhang, S. Barlow, S. Marder and A. Kahn, N-type doping of an electron-transport material by controlled gas-phase incorporation of cobaltocene, *Chem. Phys. Lett.*, 2006, **431**, 67–71, DOI: 10.1016/j.cplett.2006.09.034.

41 R. A. Laudise, C. Kloc, P. G. Simpkins and T. Siegrist, Physical vapor growth of organic semiconductors, *J. Cryst. Growth*, 1998, **187**, 449–454, DOI: 10.1016/S0022-0248(98)00034-7.

42 J. Kloc, C. Siegrist and T. Pflaum, Springer Handbook of Crystal Growth, in *Springer Handbook of Crystal Growth*, ed. G. Dhanaraj, K. Byrappa, V. Prasad and M. Dudley, Springer Berlin Heidelberg, Berlin, Heidelberg, 2010, pp. 845–867, DOI: 10.1007/978-3-540-74761-1.

43 E. Giangrisostomi, R. Ovsyannikov, F. Sorgenfrei, T. Zhang, A. Lindblad, Y. Sassa, U. B. Cappel, T. Leitner, R. Mitzner, S. Svensson, N. Mårtensson and A. Föhlisch, Low Dose Photoelectron Spectroscopy at BESSY II: electronic structure of matter in its native state, *J. Electron Spectros. Relat. Phenom.*, 2018, **224**, 68–78, DOI: 10.1016/j.elspec.2017.05.011.

44 N. Koch, D. Pop, R. L. Weber, N. Böwering, B. Winter, M. Wick, G. Leising, I. V. Hertel and W. Braun, Radiation induced degradation and surface charging of organic thin films in ultraviolet photoemission spectroscopy, *Thin Solid Films*, 2001, **391**, 81–87, DOI: 10.1016/S0040-6090(01)00961-0.

45 B. Gieseking, T. Schmeiler, B. Müller, C. Deibel, B. Engels, V. Dyakonov and J. Pflaum, Effects of characteristic length scales on the exciton dynamics in rubrene single crystals, *Phys. Rev. B: Condens. Matter Mater. Phys.*, 2014, **90**, 205305, DOI: 10.1103/PhysRevB.90.205305.

46 F. Bussolotti, J. Yang, T. Yamaguchi, K. Yonezawa, K. Sato, M. Matsunami, K. Tanaka, Y. Nakayama, H. Ishii, N. Ueno and S. Kera, Hole-phonon coupling effect on the band dispersion of organic molecular semiconductors, *Nat. Commun.*, 2017, **8**, 173, DOI: 10.1038/s41467-017-00241-z.

47 Z. Q. Li, V. Podzorov, N. Sai, M. C. Martin, M. E. Gershenson, M. Di Ventra and D. N. Basov, Light quasiparticles dominate electronic transport in molecular crystal field-effect transistors, *Phys. Rev. Lett.*, 2007, **99**, 1–4, DOI: 10.1103/PhysRevLett.99.016403.

48 S. Ciuchi, R. C. Hatch, H. Höchst, C. Faber, X. Blase and S. Fratini, Molecular fingerprints in the electronic properties of crystalline organic semiconductors: from experiment to theory, *Phys. Rev. Lett.*, 2012, **108**, 256401, DOI: 10.1103/PhysRevLett.108.256401.

49 D. Käfer and G. Witte, Growth of crystalline rubrene films with enhanced stability, *Phys. Chem. Chem. Phys.*, 2005, **7**, 2850, DOI: 10.1039/b507620j.

50 R. C. White, C. S. Fadley, M. Sagurton and Z. Hussain, Angle-resolved x-ray photoemission from the valence bands of tungsten with high angular resolution and temperature variation, *Phys. Rev. B: Condens. Matter Mater. Phys.*, 1986, **34**, 5226–5238, DOI: 10.1103/PhysRevB.34.5226.

51 R. C. White, C. S. Fadley, M. Sagurton, P. Roubin, D. Chandesris, J. Lecante, C. Guillot and Z. Hussain, Non-direct transitions in variable-temperature angle-resolved photoemission from metals, *Phys. Rev. B: Condens. Matter Mater. Phys.*, 1987, **35**, 15.

52 S. Kasap, *Principles of Electronic Materials and Devices*, McGraw-Hill, Inc., USA, 4th edn, 2006.

53 S. Olthof, W. Tress, R. Meerheim, B. Lüssem and K. Leo, Photoelectron spectroscopy study of systematically varied doping concentrations in an organic semiconductor layer using a molecular p-dopant, *J. Appl. Phys.*, 2009, **106**, 103711, DOI: 10.1063/1.3259436.

54 M. Oehzelt, N. Koch and G. Heimel, Organic semiconductor density of states controls the energy level alignment at electrode interfaces, *Nat. Commun.*, 2014, **5**, 4174, DOI: 10.1038/ncomms5174.

55 A. Zunger and O. I. Malyi, Understanding Doping of Quantum Materials, *Chem. Rev.*, 2021, **121**, 3031–3060, DOI: 10.1021/acs.chemrev.0c00608.

56 J. Li, I. Duchemin, O. M. Roscioni, P. Friederich, M. Anderson, E. Da Como, G. Kociok-Köhn, W. Wenzel, C. Zannoni, D. Beljonne, X. Blase and G. D'Avino, Host dependence of the electron affinity of molecular dopants, *Mater. Horiz.*, 2019, **6**, 107–114, DOI: 10.1039/c8mh00921j.

57 S. Hammer, C. Zeiser, M. Deutsch, B. Engels, K. Broch and J. Pflaum, Spatial Anisotropy of Charge Transfer at Perfluoropentacene-Pentacene (001) Single-Crystal Interfaces and its Relevance for Thin Film Devices, *ACS Appl. Mater. Interfaces*, 2020, **12**, 53547–53556, DOI: 10.1021/ACSAMI.0C17152/SUPPL_FILE/AM0C17152_SI_001.PDF.

58 H. Ding and Y. Gao, Electronic structure at rubrene metal interfaces, *Appl. Phys. A: Mater. Sci. Process.*, 2009, **95**, 89–94, DOI: 10.1007/S00339-008-5038-5/METRICS.